Journal of Molecular Spectroscopy 251 (2008) 268–281

Contents lists available at ScienceDirect

Journal of Molecular Spectroscopy

journal homepage: www.elsevier.com/locate/jms

N_2-, O_2- and air-broadened half-widths and line shifts for transitions in the ν_3 band of methane in the 2726- to 3200-cm^{-1} spectral region ☆

Bobby K. Antony [a], Danielle L. Niles [a], Sarah B. Wroblewski [a], Caitlin M. Humphrey [a], Tony Gabard [b], Robert R. Gamache [a,*]

[a] Department of Environmental, Earth & Atmospheric Sciences, University of Massachusetts Lowell, University of Massachusetts School of Marine Sciences, The Olney Science Center, Room 201, 265 Riverside Street, Lowell, MA 01854-5045, USA
[b] Institut Carnot de Bourgogne, UMR 5209 CNRS, Universite de Bourgogne, Faculte des Sciences Mirande, B.P. 47 870, F-21078 Dijon Cedex, France

ARTICLE INFO

Article history:
Received 20 December 2007
In revised form 22 February 2008
Available online 30 March 2008

Keywords:
Complex Robert–Bonamy formalism
Half-width
Line shift
Spectral lines
CH_4
Broadening
Temperature dependence of half-width

ABSTRACT

Complex Robert–Bonamy calculations of the pressure-broadened half-width and the pressure-induced line shift are made for some 4000 transitions in the ν_3 band of methane with N_2, O_2, and air as the perturbing gases. This work focuses on *A* and *F* symmetry transitions in the spectral range 2726 to 3200 cm^{-1}. More work is needed on the intermolecular potential before calculations can be made for the *E*-symmetry transitions. The calculations are made at 225 and 296 K in order to determine the temperature dependence of the half-width. The calculations are compared with measurements. These data are to support remote sensing of the Earth and Titan atmospheres.

1. Introduction

The Earth system is complex with many cause-and-effect relationships between land, ocean, and atmosphere. Methane, like CO_2, is present in the terrestrial atmosphere in trace amounts, but these two greenhouse gases are thought to be major drivers of climate change and global warming. There is evidence linking surface temperature changes to greenhouse gas concentrations [1,2] and there is growing evidence that climate can change much faster than previously thought [3,4]. To understand these processes and predict the future condition of the atmosphere, scientists utilize global climate models, for which the concentrations of the greenhouse gases are part of the input. The role of the gases in determining climate is complex and depends on many variables. As such, these climate models must be validated through accurate measurements. Various spectroscopic instruments such as those in orbit [5–15] provide these on a global scale providing much needed data for models [16]. In addition, a number of balloon-borne and ground-based instruments [17–24] provide data on a local scale. In this work the focus is on methane, for which the vibration–rotation bands between 9 and 1.6 μm are commonly used to monitor concentrations. A major component in the error budget of atmospheric retrievals for methane in the lower troposphere arise from the poor accuracies of the pressure-broadening coefficients.

In addition to the terrestrial atmosphere, methane is also a minor constituent of the atmospheres of other outer planets and Titan, a satellite of Saturn. Nitrogen-broadening of methane is important since the atmosphere of Titan is 90% N_2 with CH_4 being the second most abundant molecule. The Composite Infrared Spectrometer (CIRS) onboard the Cassini orbiter of the Cassini–Huygens mission to Saturn and Titan has measured the composition profile of methane on Titan [25,26] as well as the temperature profile using the ν_4 lines of methane. The CIRS instrument also measured methane on Jupiter [27] during a pass by on its voyage to Saturn.

The interpretation of remote sensing measurements, the retrieval of temperature and concentration profiles, and the study of radiative properties of the atmosphere from these remote sensed data are modeled using the absorption coefficients of atmospheric gases. The absorption coefficients, in turn, can be determined from knowledge of spectral parameters of the gases present. Of the spectral parameters, the half-widths and line shifts are the least

☆ The authors dedicate this work to Ed Cohen and Herb Pickett, two exceptional scientists and people. I (R.R.G.) am grateful for the many discussions and collaborations that I have had with Ed and Herb through the years. My interaction with them has made my life scientifically and personally richer. We wish them the very best in retirement.

* Corresponding author. Fax: +1 978 934 3069.
E-mail address: Robert_Gamache@uml.edu (R.R. Gamache).

0022-2852/$ - see front matter © 2008 Elsevier Inc. All rights reserved.
doi:10.1016/j.jms.2008.03.012

well-known [28]. A precise knowledge of the spectral parameters of methane is very important for the infrared transmission and radiance calculations of these atmospheres. This would eventually help to correctly model the radiative forcing for climate models.

The main source of spectroscopic line parameters for methane is the HITRAN database. The 2004 HITRAN database [29] contains some 251 440 methane transitions. Table 1 lists the vibration–rotation bands of $^{12}CH_4$ between 9 and 1.6 μm with the sum of line intensities greater than $\times 10^{-20}$ cm^{-1}/(molecule cm^{-2}). Given in the table are the band, the number of transitions, the band center in cm^{-1}, the wavenumber range, and the sum of the intensities. There are over 100 000 transitions in this list. While it is not practical to measure or calculate the line parameters for all transitions, data are needed at least for the strong vibrational bands. The scope of the work needed to provide the widths and shifts of methane transition has been defined by Brown et al. [30,31].

Here, we focus on the region 2726–3200 cm^{-1}, which still contains over 25 000 transitions for $^{12}CH_4$. The dominant band in this region is the ν_3 band centered at 3018 cm^{-1}. The question of lines from weaker bands contributing in particular channels must be considered carefully. We also note that algorithms to solve the radiative transfer equations often utilize transitions ±25 cm^{-1} from the edges of the channels. This paper presents calculations for 4120 ν_3 transitions in this region.

There have been numerous half-width measurements for transitions of $^{12}CH_4$ with N_2 [24,32–49] O_2, [32,42,44,45,48,49] air [32,36,38,40,42,43,45,50–53], CH_4 [32,34,36,39,44,48,49,54–60], and other molecules/atoms [32,33,37,39,41,42,44,46–48,54,56,58,61] as the buffer gas. These data are summarized in Table 2. From these studies insight has been gained on the dependence of the half-width and line shift on a number of variables. The vibrational dependence of the half-width [40,44,45,51–53,58,60] has been found to be small. In an early study, Pine [44] reports that "within experimental error…there appears to be little or no vibrational, branch, or carbon isotope dependence to the infrared broadenings of methane." Later studies [45,53,60] found the vibrational dependence of the half-width to be of order a few percent for low J lines, but can be of order 20% for high J lines. Predoi-Cross et al. [53,60] also found that bands with only the F2 vibration symmetry had similar widths at lower J'' but became noticeably different by $J'' = 10$. However, the bands with more vibrational components like $\nu_1 + \nu_2$ ($F1 + F2$) had different patterns in the widths and $\nu_3 + \nu_4$ had no pattern at all. If the average values are considered, the differences are generally less than 5%. Some studies have focused on the dependence of the half-width on the rotational quantum number, J'', [40,44,45,51–53,60] and branch label, P, Q, or R, [40,45,46,51–53,60]. They report that the half-widths decrease with J'' but there is no simple propensity rule to describe the behavior and the branch dependence is small; of order a few percent. A number of these studies [40,44–46,51–53,59–61] have considered the dependence on the symmetry of the transition, A, E and F. In general the F-symmetry transitions are the largest and the E-symmetry are the smallest, however Predoi-Cross et al. [53] found this not to be true for the $\nu_3 + \nu_4$ and the $\nu_2 + \nu_3$ bands, and Devi et al. [51] found all three symmetry level transitions have almost the same average pressure-broadening coefficient. Pine et al. [44,46,47] considered the dependence on various line shape models (a few percent difference (see also Mondelain et al. [24])) and on the order index N, which, for lines of the same ΔJ, J'', C but different N, the widths are slightly different and they shows a decrease for F-symmetry transitions and an increase for E-symmetry transitions. Finally a number of these studies have considered the dependence on the perturbing molecule/atom [38,40,44–48,61] and have calculated the ratio of the half-width for the same rovibrational transition for different broadening species. Pine et al. [44,46–48] report the ratios as being somewhat constant, indicating that predictions for other perturbers can be obtained once the ratio of one transition is known.

Less study of the line shift has been done, in part due to the difficulty of these measurements. Still the studies of air [40,42,43,45,51–53], N_2 [42–48], O_2 [44,45,48], Self [44,48,54,57,60], and other atom/molecule [42,44,46–48,54,61] pressure induced shifts of methane amount to several thousand transitions for some 10 different vibrational bands (see Table 2). The shifts demonstrate a marked dependence on vibrational band. From the studies made the results indicate that most of the shifts are negative and transition dependent.

The temperature dependence of the half-width has been considered in a number of studies [24,34,35,39,41–43,50,52]. These measurements are summarized in Table 3. An early study [50] based on three lines suggested a temperature dependence that varied with the symmetry (A or F) of the transition. However, later studies involving many more transitions [43,52] show much variation and overlap of the temperature exponents for A-, E-, and F-symmetry transitions. The later studies found the smallest values of n occurred for E-symmetry lines and that lines with large half-widths also have large n values. Smith et al. [43] also comment that the scatter among values for the same symmetry species for a single m (branch-J label) represent real differences between transitions involving different sublevels. In a study of approximately 370 transitions Devi et al. [52] state the variation of n with the branch-J label m is not so apparent. Their results indicate a similar

Table 1
Vibration–rotation bands of $^{12}CH_4$ between 9 and 1.6 μm with the sum of line intensities greater than $\times 10^{-20}$ cm^{-1}/(molecule cm^{-1})

Band	No. of lines	Band center (cm^{-1})	ω_{min} (cm^{-1})	ω_{max} (cm^{-1})	Σ line intensities
$2\nu_4 - \nu_4$	8933		928.620	1676.111	3.76×10^{-20}
$\nu_4 -$ gs	5303	1310.7606	943.985	1640.788	5.09×10^{-18}
$\nu_2 -$ gs	3246	1533.3367	1302.815	1845.791	5.38×10^{-20}
$2\nu_4 -$ gs	6700	2612	2097.844	3229.470	5.49×10^{-20}
$\nu_2 + \nu_4 -$ gs	9291	2830	2455.981	3276.448	3.72×10^{-19}
$2\nu_2 -$ gs	3590	3062	2703.282	3476.183	3.17×10^{-20}
$\nu_3 -$ gs	6183	3018.9205	2706.564	3277.552	1.08×10^{-17}
$\nu_3 + \nu_4 - \nu_4$	3126	3010	2828.821	3274.337	5.32×10^{-20}
$\nu_2 + \nu_3 - \nu_2$	2053	3010	2836.583	3159.447	1.13×10^{-20}
$3\nu_4 -$ gs	8631		3354.842	4459.426	3.27×10^{-20}
$\nu_2 + 2\nu_4 -$ gs	11614		3712.594	4735.223	3.41×10^{-20}
Unassigned	3274		3841.018	6184.492	7.48×10^{-20}
$\nu_1 + \nu_4 -$ gs	3184	4223.497	3873.714	4507.039	2.53×10^{-19}
$\nu_3 + \nu_4 -$ gs	11247	4340	3960.814	4608.955	4.75×10^{-19}
$2\nu_2 + \nu_4 -$ gs	9676		4011.160	4727.670	2.42×10^{-20}
$\nu_2 + \nu_3 -$ gs	6910	4540.	4310.318	4809.453	7.17×10^{-20}
$2\nu_3 -$ gs	144	6004.991	5891.065	6106.284	5.97×10^{-20}

Table 2
Measurements of half-widths and line shifts of methane transitions

Ref.	Perturbing gases	Parameters	No. of lines	Range cm^{-1}	J''	Band
[55]	Self	γ	1	2947.88	21	$\nu_2 + \nu_4$
[54]	Self, Xe	γ, δ	1	—	7	ν_3
[57]	Self	γ, δ	27	9080–9130	0–7	$3\nu_3$
[56]	Self, H_2	γ	4	—	0–4	$2\nu_3$
[32]	H_2, He, N_2, O_2, air	γ	10	3036–3185	1–16	ν_3, $2\nu_3$
[58]	Self, H_2, He	γ	9	1207–1322	1–20	ν_4
[50]	Air	γ and Tdep	3	—	0–2	ν_3
[36]	Self, N_2, air	γ	5	1586–1590	4	ν_2
[34]	Self, N_2	γ and Tdep	7	2870–2883	14	ν_3, $\nu_2 + \nu_4$
[35]	N_2	γ and Tdep	77	1299–1354	—	ν_4
[38]	Air, N_2	γ	25	1256–1348	0–11	ν_4
[37]	N_2, H_2, He	γ	7	9030–9120	0–6	$3\nu_3$
[39]	Self, N_2, H_2, He	γ and Tdep	2	6196.83 and 6818.84 Å	—	$6\nu_1$, $5\nu_3$
[59]	Self	γ	61	1310–1370	0–12	ν_4
[40]	Air, N_2	γ	294	1168–1678	0–18	ν_4,ν_2
[33]	Ar, He, H_2, N_2	γ	9	—	1–6	$3\nu_3$
[61]	Ar	γ, δ	118	1228–1371	0–12	ν_4
[41]	H_2, N_2, Ar, He	γ and Tdep	11	1270–1316	0–9	ν_4
[42]	He, Ne, Ar, H_2, N_2, O_2, air	γ and Tdep, δ and Tdep	6	1332–1348	4–7	ν_4
[43]	Air, N_2	γ and Tdep, δ and Tdep	148	1210–1371	0–12	ν_4
[44]	Self, N_2, O_2, H_2, Ar, He	γ, δ	66	3012–3018	1–13	ν_3
[51]	Air	γ, δ	270	4138–4600	0–11	$\nu_1 + \nu_4$, $\nu_3 + \nu_4$, $\nu_2 + \nu_3$
[45]	Air, N_2, O_2	γ, δ	~450	2842–3061	0-17	$\nu_3, \nu_2 + \nu_4, 2\nu_4^2, 2\nu_2^2$,
[52]	Air	γ and Tdep, δ and Tdep	~740	4118–4615	0–12	$\nu_1 + \nu_4$, $\nu_3 + \nu_4$, $\nu_2 + \nu_3$
[46]	N_2, Ar	γ, δ	102	2916–3123	0–10	ν_3
[47]	N_2, Ar	γ, δ	102	2917–3028	0–10	ν_3
[48]	H_2, He, N_2, O_2, Ar, self	γ, δ	66	3012–3019	1–13	ν_3
[49]	Self, N_2, O_2	γ, δ	4	2914–2922	4–7	$\nu_2 + \nu_4$
[60]	Self	γ	1423	4100-4635	0-16	$\nu_2 + 2\nu_4$, $\nu_1 + \nu_4$, $\nu_3 + \nu_4$, $2\nu_2 + \nu_4$, $\nu_2 + \nu_3$
[53]	Air	γ	1011	4100-4635	0-16	$\nu_2 + 2\nu_4$, $\nu_1 + \nu_4$, $\nu_3 + \nu_4$, $2\nu_2 + \nu_4$, $\nu_2 + \nu_3$
[24]	N_2	γ	4	2926–2928	9	ν_3

Table 3
Measurements of temperature dependence of half-widths and line shifts

Reference	Parameter	Perturbing gas	No. of lines	Temperature range (K)	Band
[50]	γ	Air	3	200–300	ν_3
[35]	γ	N_2	77	153–200	ν_4
[34]	γ	Self, N_2	5	215–297	ν_3, $\nu_2 + \nu_4$
[39]	γ	Self, N_2, H_2, He	2	77–295	$6\nu_1$, $5\nu_3$
[41]	γ	H_2, N_2, He, Ar	6	130–295	ν_4
[42]	γ, δ	He, Ne, Ar, H_2, N_2, O_2, air	6	161–295	ν_4
[43]	γ, δ	Air, N_2	148	210–314	ν_4
[52]	γ, δ	Air	370	212–97	$\nu_1 + \nu_4$, $\nu_3 + \nu_4$, $\nu_2 + \nu_3$
[24]	γ	N_2	4	90–96	ν_3

situation for n with respect to vibrational dependence but n does seem to be symmetry dependent.

For the perturbing gases of interest here, N_2, O_2, and air, the measured range of the temperature exponents is ~1.1 to 0.37 and ~0.88 to 0.15 for air- and N_2-broadening, respectively. For O_2-broadening there are not as many measurements but where there are the O_2- and N_2-broadening results are similar. A number of the studies that considered a number of perturbing gases [39,41,42] found n to vary considerably as a function of the perturbing gas. Most of these studies used the power law form of the temperature dependence of the half-width (see Eq. (10) below). Mondelain et al. [24] also fit their results in ln–ln space by a second order polynomial and noted improved results.

Despite the number of experiments performed to determine the line shape parameters for several thousands of methane transitions broadened by air, nitrogen, oxygen, CH_4, and other perturbing molecules/atoms, parameters for many thousands of other transitions are still unknown. A theoretical model with adequate accuracy will be valuable to complement the experimental endeavors. Presently we have used the mean-relative thermal velocity approximation to the complex Robert–Bonamy (CRB) formalism [62,63] to determine the line shape parameters, half-width and line shift, for methane transitions. The CRB formalism has been very successful in predicting the half-width and line shift for self- and foreign-broadened spectral lines of many molecular systems [64–70]. For this work, calculations for N_2- and O_2-broadened half-width and line shift for 4120 methane transitions in the spectral region of 2706–3200 cm^{-1} at temperatures 225 and 296 K were made. Air-broadening of methane is obtained from the N_2- and O_2-broadening calculations. From these calculations the temperature dependence of the half-width was determined. We have compared the results with available experimental values.

2. Theory

2.1. General theory

The complex implementation of the Robert–Bonamy formalism [62] has been used to determine the pressure broadened half-width and line shift for methane transitions. Further details on

the theory and its derivations may be obtained from [63,71,72] and references therein. In this article we have presented only the necessary equations and the salient features of the method. The present approach yields the half-width and line shift for a ro-vibrational transition $f \leftarrow i$ given by the real and imaginary part of the expression,

$$(\gamma - \mathrm{i}\delta)_{f\leftarrow i} = \frac{n_2 v}{2\pi c}\left\langle \left[1 - \mathrm{e}^{-{}^{R}S_2(f,i,J_2,v,b)}\mathrm{e}^{-\mathrm{i}\left[{}^{I}S_1(f,i,J_2,v,b)+{}^{I}S_2(f,i,J_2,v,b)\right]}\right]\right\rangle_{bJ_2} \quad (1)$$

where, n_2 is the number density of perturbers and $\langle\ldots\rangle_{bJ_2}$ is the average over all trajectories (with impact parameter b) and initial rotational state J_2 of the collision partner. Note that Eq. (1) is the mean relative thermal velocity approximation (MRTV) to the CRB formalism. The real S_1 and complex $S_2 = {}^{R}S_2 + i^{I}S_2$ are the first- and second-order terms in the expansion of the scattering matrix. S_1 and S_2 depend on the ro-vibrational states (and the associated collision-induced transitions between these levels), the intermolecular potential and the collision dynamics involved. The complete expressions for these terms are explicitly defined in Refs. [62,63,71,72].

Several important features have been incorporated in the present CRB formalism; (i) the imaginary components have been retained, (ii) the elimination of the cut-off procedure, (iii) and the better modeling of close collisions. In many applications of the theory the imaginary parts are not used and only the approximate half-width calculated. Here the S_1 and ${}^{I}S_2$ terms are retained and the half-width and line shift are determined from a single calculation. The cut-off procedure adopted by earlier theories [73,74] was eliminated by the use of linked-cluster techniques [75]. The close intermolecular collisions (small b) are now better defined by (a) the dynamics, which is second order in time producing curved trajectories based on the isotropic part of the intermolecular potential, and (b) the short-range (Lennard–Jones) atom–atom potential, which is an important component for a proper description of pressure broadening, especially in the case of weekly interacting molecules [64].

2.2. The potential

The term S_1, a purely imaginary part of Eq. (1), is isotropic in the absence of any vibrational dependence of the anisotropic intermolecular forces. It has the label of the vibrational dephasing term and arises only for transitions where there is a change in the vibrational state. The potential leading to S_1 is given in terms of the London dispersion interactions given as,

$$V_{\mathrm{iso}}^{\mathrm{dispersion}} = -\frac{3}{2}\frac{I_1 I_2}{I_1 + I_2}\frac{\alpha_1\alpha_2}{R^6} \quad (2)$$

where α_k and I_k are the polarizability and ionization potential of the radiator ($k = 1$) and perturber ($k = 2$). The vibrational dependence of the polarizability, α_k, is given by Raynes et al. [76] (in a.u.) as,

$$\alpha = \alpha_0 + \sum_j b_j v_j \quad (3)$$

with v_j the number of quanta in the nth normal mode and the coefficients $b_1 = 0.189$, $b_2 = 0.124$, $b_3 = 0.333$ and $b_4 = 0.080$ (all in units of a_0^3).

The complex valued $S_2 = {}^{R}S_2 + i^{I}S_2$ results from the anisotropic interaction potential with leading electrostatic components and atom–atom terms. The atom–atom potential is defined as the sum of pairwise Lennard–Jones (6–12) [77] interactions between atoms of the radiating and perturbing molecules given by,

$$V^{\mathrm{at-at}} = \sum_{i=1}^{n}\sum_{j=1}^{m} 4\varepsilon_{ij}\left\{\frac{\sigma_{ij}^{12}}{r_{1i2j}^{12}} - \frac{\sigma_{ij}^{6}}{r_{1i2j}^{6}}\right\} \quad (4)$$

where n and m are the number of atoms in molecules 1 and 2 and the subscripts $1i$ and $2j$ stands for the ith atom of molecule 1 and jth atom of molecule 2, respectively. The ε_{ij} and σ_{ij} are the Lennard–Jones parameters for the atomic pairs. The heteronuclear atom–atom parameters are constructed from the homonuclear atom–atom parameters (ε_i and σ_j) by the combination rules of Hirschfelder et al. [78] or Good and Hope [79]. The atom–atom distance r_{ij} is expressed as an expansion of the inverse of center of mass separation, R given by Sack [80]. As this expansion is truncated, sufficient order must be taken to ensure the convergence of calculated half-widths and line shifts [81] (more on this below).

The reduced matrix elements are evaluated using the interacting band wavefunctions described below. These wavefunctions are more accurate than the previously used isolated band wavefunctions [64], particularly at high J where the states from different bands are often overlapping. The wavefunctions are complete up to $J = 30$, enabling us to study methane transitions up to $J = 28$.

Most of the molecular parameters used here for the system are well known and we have used the best available values from the literature. The multipole moments, rotational constants, polarizability and ionization potential (IP) employed here are tabulated in Table 4.

2.3. Energies and wavefunctions for methane

The eigenfunctions for methane were calculated using the tetrahedral formalism adapted to rotation–vibration quantum states of spherical top molecules [82,83]. Whatever the vibrational states of interest, these functions are obtained from a numerical diagonalization of an effective Hamiltonian. The matrix elements of this Hamiltonian between symmetry adapted basis functions are derived using standard tensorial techniques. Any wavefunction may be written

$$|J_g CN\sigma\rangle = \sum U^{(J,C,N)}_{n_r,C_r,\{v\},C_v}|J_g; n_r; C_r; \{v\}, C_v; CN\rangle \quad (5)$$

where J is the total angular momentum (of g parity in the full rotation group) and C is the symmetry species. $C = A_1$, A_2, E, F_1, or F_2 in the T_d point symmetry group. N is the order index and numbers the eigenstates at fixed polyad, J and symmetry species in increasing energy order. σ stands for one of the components for a given symmetry species, if the dimension of C is greater than one. Energies are always degenerate with respect to σ. U is the unitary transformation that diagonalizes the Hamiltonian, while n_r and C_r are indices for rotational basis functions and $\{v\}$ and C_v are indices for vibrational ones. Coupled rotation–vibration basis functions are of C symmetry. $\{v\}$ contains the set of vibrational indices that identifies a given polyad. In short, polyads are groups of vibrational states

Table 4
Molecular constants for methane, nitrogen and oxygen

Mol	Multipole moments		Rotational constant (cm^{-1})		Polarizability (10^{-26} cm^3)		IP (eV)	
CH_4	$\Omega = 2.6 \times 10^{-34}$ esu cm^3	[100]					12.598	[101]
	$\sigma = 4.8 \times 10^{-42}$ esu cm^4	[102]						
N_2	$\theta_{zz} = -1.3 \times 10^{-26}$ esu cm^2	[103]	2.007	[104]	17.4	[105]	15.576	[106]
O_2	$\theta_{zz} = -0.4 \times 10^{-26}$ esu cm^2	[107]	1.438	[104]	15.8	[105]	12.063	[101]

arising from the near degeneracy between the four vibrational fundamentals,

$$\sigma_1 \approx 2\sigma_2 \approx \sigma_3 \approx 2\sigma_4 \tag{6}$$

Thus, when calculating energies and eigenstates, an effective Hamiltonian is built for each polyad. It is effective in the sense that a contact transformation has been applied to the initial Hamiltonian to make it block diagonal with respect to polyads. In order of increasing wavenumbers, the lowest polyads are the ground state, denoted P_0, the dyad $\{v_2, v_4\}$, denoted P_1 and the pentad $\{v_1, 2v_2, v_2 + v_4, v_3, 2v_4\}$, denoted P_2. The present study is concerned with P_0 and P_2. The eigenvalues and the eigenfunctions for the effective Hamiltonians were calculated up to $J = 30$. We describe below how these symmetry-adapted wavefunctions were subsequently expressed in the classical basis, related to the O(3) full rotation group, for further use in line-broadening calculations.

2.3.1. The ground vibrational state of methane

The Hamiltonian model for this state is developed up to order 6, which means that symmetry allowed rotational operators are developed up to power 8 in the individual components of the angular momentum. Wavefunctions are expressed in a classical basis through the use of the G unitary transformation [84] that applies to the rotational basis functions,

$$|J_g n_r C_r \sigma_r\rangle = \sum_K {}^{(J_g)}G^K_{n_r,C_r,\sigma_r} |J,K\rangle \tag{7}$$

In the ground state, the vibrational coupling is trivial, thus $C = C_r$ and $\sigma = \sigma_r$. In the function $|J,K\rangle$, the second projection number is omitted. In angular coordinate representation, this function is proportional to a Wigner matrix element.

2.3.2. The v_3 state of methane

The eigenstates were calculated for this vibrational state using a Hamiltonian model where all symmetry allowed vibrational couplings are accounted for (pentad scheme). The development orders are 6 for the ground states, 6 for the dyad (up to power 2 in elementary vibrational operators related to v_2 and v_4, and power 6 for rotational operators) and 4 for the pentad (up to powers 2, 3 or 4 in elementary vibrational operators, and powers 2, 3 or 4 for rotational operators). This procedure is known to be more accurate than calculating eigenstates for the v_3 state alone (isolated band scheme). For instance, an isolated band model for v_3 may be appropriate for low J values, say $J < 10$. At higher J values, energy levels from neighboring vibrational states begin to cross each other, and the accuracy of the isolated band model degrades rapidly. As a consequence, the eigenfunctions for v_3 are developed on basis functions related not only to v_3 itself, but also on basis functions for other vibrational states in the same polyad. Nevertheless, the v_3 wavefunctions can be considered to belong to the v_3 vibrational states at 80 % or more, from inspection of the numerical results. In order to express these functions with classical notations, only the parts of the eigenfunctions that develop upon v_3 basis functions are kept. Obviously, these modified functions are re-normalized after truncation. Then, a basis transformation is done using the K isoscalar factors for the chain of groups $O(3) \supset T_d$ [82] to extract the so-called R-pure rotational quantum number. This is done by introducing the $\lambda_3 = 1$ vibrational angular momentum (u parity in the O(3) group) associated to v_3. After this step, the basis functions are expressed in the $|R,K_R\rangle$ classical basis, KR being the projection number of the R momentum, using the G unitary transformation again. These basis transformations are written as

$$|J_g; n_r; C_r; \{v_3\}, F_2; C\sigma\rangle = \sum_{R,n_R,K_R} K^{(J_g 1_u R_u)}_{(n_r C_r 0 F_2 n_R C)} {}^{(R_u)}G^{K_R}_{n_r,C,\sigma} |(J_g, 1_u), R_u, K_R\rangle. \tag{8}$$

In the function $|(J_g, 1_u) R_u, K_R\rangle$, the second projection number is omitted again since the basis transformation acts only in the molecule fixed frame.

2.3.3. Matrix elements calculations

The above wavefunctions have been used to calculate the matrix elements of the angular operators appearing in the anisotropic parts of the intermolecular potential. Operators for the close distance (atom–atom) potential and the electrostatic one are the same. In classical notations, these operators are labeled by a tensorial rank, λ, in the rotation group and the associated projection number k. Matrix elements are obtained with standard techniques based on the Wigner–Eckart theorem. Expressions for these elements were given previously [64]. In using strictly classical notations related to rotation groups, all non-vanishing matrix elements would need to be calculated. We note, however, that in the T_d point group, the particular combinations of angular operators for methane may be labeled with symmetries A_1 or A_2 [85,86]. This property arises from the fact that A, E, and F type states of methane do not mix through collisional processes. Thus, the amount of matrix elements to be calculated can be restricted to the only relevant ones, that is, for A type, E type, or F type states but not between states of different types.

3. Calculations

In this work we focus on the strongest band (i.e. the v_3 band) in the region cited above. The data for the band were extracted from the 2004 HITRAN database [29]. In the present work it is found that convergence of the atom–atom part of the intermolecular potential is obtained at 12th order for transitions involving A and F symmetries. However, for E-symmetry transitions the results show that the calculations are not converged even at 14th order of expansion. Since it is the current limit of the codes, results for E-symmetry transitions are not reported here. This problem is currently being investigated. From the remaining A- and F-symmetry transitions we were able to make calculations for 524 A-symmetry transitions and 3596 F-symmetry transitions. The present calculations do not take into account any line-coupling effects. However, Predoi-Cross et al. [87], in a study of the $v_2 + v_3$ band of methane, state the addition of line mixing in the multispectral fit changed half-widths by a small amount (0.5%) and changed line shifts (both self- and air-shifts) by 7–20%.

Preliminary calculations: It is known that the combination rules used to determine the atom–atom parameters are suspect and the resulting coefficients have large uncertainty [79]. An initial calculation of the 52 A- and F-symmetry transitions for which Pine [44] made N_2- and O_2-broadening measurements was done yielding −8.8% and 15.0% difference, respectively, between calculations and measurement. To adjust the atom–atom parameters six transitions (1 A- and 5 F-species) and five F-symmetry transitions were chosen for N_2- and O_2-broadening, respectively, such that adjusting the atom–atom coefficients for these lines would rescale the average difference with Pine's 1992 measurements [44] to near zero; these transitions are shown in Table 5. The initial and final atom–atom parameters are shown in Table 6. With these parameters the average percent difference when comparing with Pine's data are 0.15 and −2.1 for N_2- and O_2-broadening, respectively.

Calculations of half-widths and line shifts were performed using the mean relative thermal velocity approximation to the CRB formalism for the CH_4–N_2 and CH_4–O_2 systems for the A- and F-symmetry transitions in the v_3 band at 296 and 225 K. The atom–atom potential is expanded to 12th order and the imaginary components (i.e. a complex calculation) are used.

Table 5
Transitions used to adjust atom–atom coefficients

N_2-broadening	O_2-broadening
2 *F*1 8 ← 2 *F*2 1	8 *F*1 30 ← 8 *F*2 1
9 *A*1 11 ← 9 *A*2 1	9 *F*2 34 ← 9 *F*1 2
10 *F*1 38 ← 10 *F*2 3	10 *F*1 37 ← 10 *F*2 2
11 *F*2 42 ← 11 *F*1 3	10 *F*2 39 ← 10 *F*1 1
12 *F*2 47 ← 12 *F*1 3	12 *F*1 46 ← 12 *F*2 3
12 *F*1 45 ← 12 *F*2 2	

Table 6
Initial and final atom–atom parameters

Pair	ε/k_B (K)		σ/(Å)	
	Initial	Final	Initial	Final
H–N	20.50	20.50	3.00	2.85
C–N	34.30	32.59	3.45	3.45
H–O	24.15	24.15	2.84	2.70
C–O	40.43	38.01	3.28	3.02

For air-broadening of methane, the half-width and line shift were obtained assuming binary collisions and Dalton's law,

$$\gamma_{air} = 0.79\gamma_{N_2} + 0.21\gamma_{O_2} \quad (9)$$

and

$$\delta_{air} = 0.79\delta_{N_2} + 0.21\delta_{O_2}.$$

Eqs. (9) are used to find the air-broadened half-width and shift at both temperatures. From the data at each temperature, the temperature dependence of the half-width is determined by the power law model,

$$\gamma(T) = \gamma(T_0)\left[\frac{T_0}{T}\right]^n, \quad (10)$$

where T_0 was set to 296 K and n is called the temperature exponent.

4. Results and discussion

The calculations provide the half-width, line shift, and temperature dependence of the half-width for N_2-, O_2-, and air-broadening of ν_3 transitions of methane with $J \leqslant 28$ in the 2726- to 3200-cm^{-1} spectral range. Wherever possible the calculations are compared with measurement. The dependence of the half-width on the rotational quantum numbers and on temperature are also discussed. The analysis was carried out for N_2-, O_2-, and air-broadening of the methane transitions.

4.1. Dependence of the half-width and line shift on rotational states

Calculations of the half-width and line shift provide data for 524 *A*-symmetry transitions and 3596 *F*-symmetry transitions in the ν_3 band with $J \leqslant 28$. Table 7 presents the range of values for the half-width, line shift, and temperature dependence of the half-width (temperature exponent) for N_2-, O_2-, and air-broadening of methane. There are several interesting facts that come from this table. These data show that the oxygen-broadened half-widths are similar to the nitrogen-broadened half-widths, in fact the minimum O_2-broadening values is greater than the minimum N_2-broadening value. This fact was first pointed out to one of the authors (R.R.G.) by Devi [88] in 1988. The later publication [89] showed that the oxygen-broadened values are sometimes larger than the nitrogen-broadened values. Note, the work of Devi et al. was for transitions in the ν_3 band of the carbon-13 isotopolog of methane, however that should not have a great effect (a few percent) on the half-widths. Here, the half-widths range from small values of 0.017 cm^{-1} atm^{-1} to roughly 0.065 cm^{-1} atm^{-1}. There is not a great amount of variation in the magnitude of the half-width as a function of the perturbing molecules studied here. The large difference in the quadrupole moments of N_2 and O_2 suggests that the CH_4–N_2 and CH_4–O_2 collision systems are not dominated by the electrostatic part of the intermolecular potential. This fact was proved by Neshyba et al. [64] in a theoretical study of transitions in the ν_3 band of methane broadened by N_2. In their work they showed that the atom–atom part of the intermolecular potential is dominant, giving results an order of magnitude larger than the electrostatic potential calculation, which explains why early Anderson–Tsao–Curnutte-type calculations [90] needed to scale the electrostatic moments of methane to get reasonable results.

The data were analyzed for structure with respect to quantities describing the transitions. The rotational states of methane are described by the rotational quantum number *J*, the symmetry, and the counting (order) index, *N* [31]. In Fig. 1 the air-broadened half-width is plotted versus J'' for Q- (top panel), R- (middle panel), and P-branch (bottom panel) transitions. *F*-symmetry transitions (solid triangles) are plotted at J'' and *A*-symmetry transitions (open circles) are shifted to $J'' + 0.3$ to make identification easier. First, there does not seem to be a great difference in the half-widths as a function of the branch or as a function of the symmetry of the transition. As J'' increases, the number of states increases allowing more transitions for a given J''. The plot shows that as J'' increases the spread in the values of the half-width for a given J'' increases dramatically; at $J'' = 10$ the spread is roughly from 0.05 to 0.06 cm^{-1} atm^{-1} and by $J'' = 28$ the spread is from just under 0.02 to about 0.055 cm^{-1} atm^{-1}. CH_4–air, CH_4–N_2, and CH_4–O_2 are not molecular pairs where resonant collisions dominate. Thus, the small values seen in the plot indicate that for many transitions off-resonance effects will be important.

Because of the large number of methane transitions, scientists often must attempt to predict half-widths for transitions from half-widths of lines with different symmetry, perturbing species, quantum numbers, etc. Fig. 1 shows that *A*- and *F*-symmetry transitions appear similar. Is it possible to predict half-widths for *A*-/*F*-species transitions from *F*-/*A*-species transitions with the same quantum numbers? To address this question the calculated data for N_2-broadening were taken and ratios of *A*-symmetry transition divided by the corresponding *F*-symmetry transition were calculated. The pairs of lines are chosen such that the upper and lower rotational quantum numbers are the same, the *A*1 symmetry is paired with the *F*1 symmetry and the *A*2 symmetry is paired with the *F*2 symmetry, the lower order index values are the same. Because the allowed order index for *A*- and *F*-symmetry states are quite different, the pairs were created from the minimum N' and for the maximum N' of each symmetry species. For example the line $J'A1N'_{min} \leftarrow J''A2N''$ is paired with $J'F1N'_{min} \leftarrow J''F2N''$. The

Table 7
Minimum and maximum values of the half-width, line shift, and temperature dependence of the half-width (temperature exponent) for N_2-, O_2-, and air-broadening of methane

Perturber	γ_{min} (cm^{-1} atm^{-1})	γ_{max} (cm^{-1} atm^{-1})	δ_{min} (cm^{-1} atm^{-1})	δ_{max} (cm^{-1} atm^{-1})	n_{min}	n_{max}
N_2	0.0169	0.0657	−0.0208	0.0009	−0.546	0.759
O_2	0.0251	0.0606	−0.0194	−0.0004	−0.047	0.752
Air	0.0186	0.0646	−0.0205	0.0006	−0.398	0.757

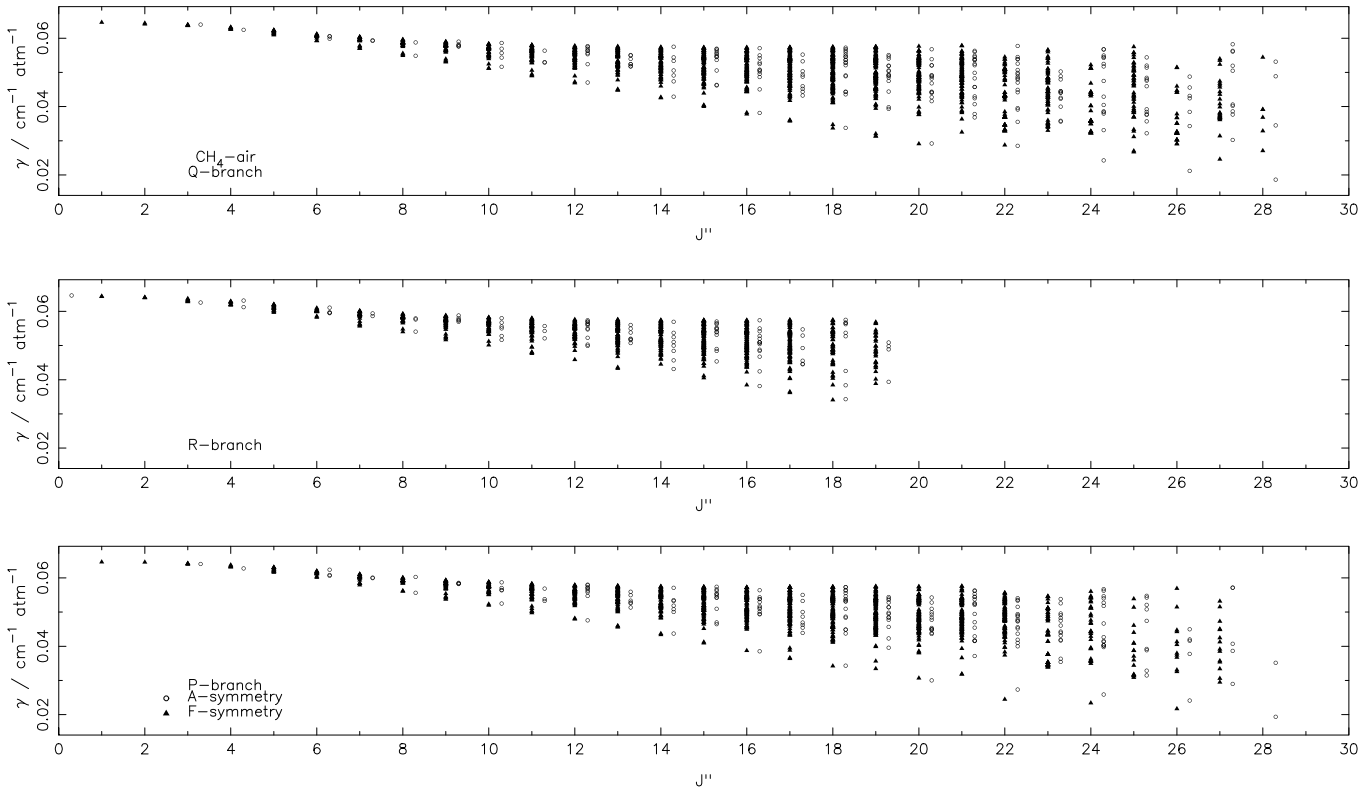

Fig. 1. Calculated air-broadened half-widths of CH_4 versus J''. (Top) Q-branch lines, (middle) R-branch lines, (bottom) P-branch lines, F-symmetry transitions are solid delta symbols and A-symmetry transitions are open circles. A-symmetry points are plotted at $J''+0.3$.

ratios are plotted versus J'' for Q-branch (top panel), R-branch (middle panel), and P-branch (bottom panel) lines in Fig. 2. In the figure, open circles correspond to $C''=A1$ transitions and solid triangles to $C''=A2$ transitions. For J'' less than 10 the ratios are close to one but the spread increases as J'' increases. The values range from 0.44 to 2.1, thus one should be cautious applying such an algorithm, especially to intermediate to high J lines.

Another approach might be to use half-widths of the transitions of the same overall symmetry species to predict the other, i.e. $C''=A1$ to predict $C''=A2$, etc. Using the data for N_2-broadening of CH_4 transitions were paired as $J'A1N' \leftarrow J''A2N''$ is paired with $J'A2N' \leftarrow J''A1N''$ with a similar pairing for F-symmetry transitions. The ratios of the half-widths are plotted in Fig. 3 versus branch symbol m, where $m=J''+0.5$ for Q-branch lines, $m=J''$ for R-branch lines, and $m=-J''$ for P-branch lines. For m small the ratio is near 1, however as m increases the spread in the ratios increases greatly. The range in the ratios is from 0.4 to 2.5. Again caution should be used applying such an algorithm to lines with $J''>10$.

The large spread as J'' increases is related to the increased number of states that a given lower state can connect to. The spread suggest the upper state interactions affect the calculations. To test the effect of the upper states on the calculation, we randomly looked through the N_2-broadening data file and selected the 15 F1 1 lower state. This lower state is involved in transitions to 32 upper states; eleven 14 $F2$ states, ten 15 $F2$ states, and eleven 16 $F2$ states. Fig. 4 shows the half-width versus the order index for the upper state with R-branch lines as solid squares, Q-branch lines as open circles, and P-branch lines as solid delta symbols. The range of half-width values is from about 0.039 to 0.058 $cm^{-1}\,atm^{-1}$. Note, independent of branch, there is not a smooth variation of the half-width as a function of the order index. Thus the knowledge of the half-width for a transition will not provide a good prediction of the half-width for a transition with the same J'', J', symmetry, N'' but different N'.

One other approach that is commonly used to predict half-widths for methane transitions is to scale as a function of perturbing molecule [24]. Using the CRB calculated N_2-, O_2-, and air-broadened files, the ratios $\gamma(O_2)/\gamma(N_2)$ and $\gamma(\text{air})/\gamma(N_2)$ were determined. The ratio $\gamma(O_2)/\gamma(N_2)$ is plotted versus m in Fig. 5 where the solid triangles are F-species lines and open circles are A-species lines. The m values of the A-species lines are also shifted up in magnitude by 0.3 to make identification of the symmetry easier. Pine [44] reports the $\gamma(O_2)/\gamma(N_2)$ ratio to be 0.937 ± 0.015 from his measurements (up to $J''=13$). For $J''\leqslant 13$ the calculations give a ratio of 0.976 ± 0.022. The ratios from the CRB calculations range from 0.92 for m near 0 to 1.5 for m near 28. This plot shows that the $\gamma(O_2)$ values are larger than the corresponding $\gamma(N_2)$ values when J'' is greater than about 15. The case for the ratios $\gamma(\text{air})/\gamma(N_2)$ versus m shows that the ratio range from 0.98 at m small to 1.1 for m large. Thus scaling from N_2-broadened half-widths to air-broadened half-widths (or vise versa) should be good to ~10%. One should be cautious applying such algorithms for other perturbing molecules and for states with $J''>10$.

Table 7 shows the line shifts go from a minimum value of $\sim -0.02\,cm^{-1}\,atm^{-1}$ to small positive values of $0.0009\,cm^{-1}\,atm^{-1}$ except for the O_2-pressure-induced line shifts, which are all negative. Fig. 6 is a plot of the air-induced line shift versus J'', the open circle symbols are for A-symmetry transitions and solid Δ symbols are for the F-symmetry transitions. The A-symmetry transitions are shifted in m by 0.3 to make identification easier. The air-induced line shift data were fit to a straight line giving $\delta_{\text{air}}\ (cm^{-1}\,atm^{-1}) = -0.1262\times10^{-3}\ J'' - 0.6451\times10^{-2}$. The correlation coefficient of the fit is −0.4366. This line is shown in Fig. 6. The spread about this line does not become great until $J''>20$ where it then becomes substantial. The figure shows that al-

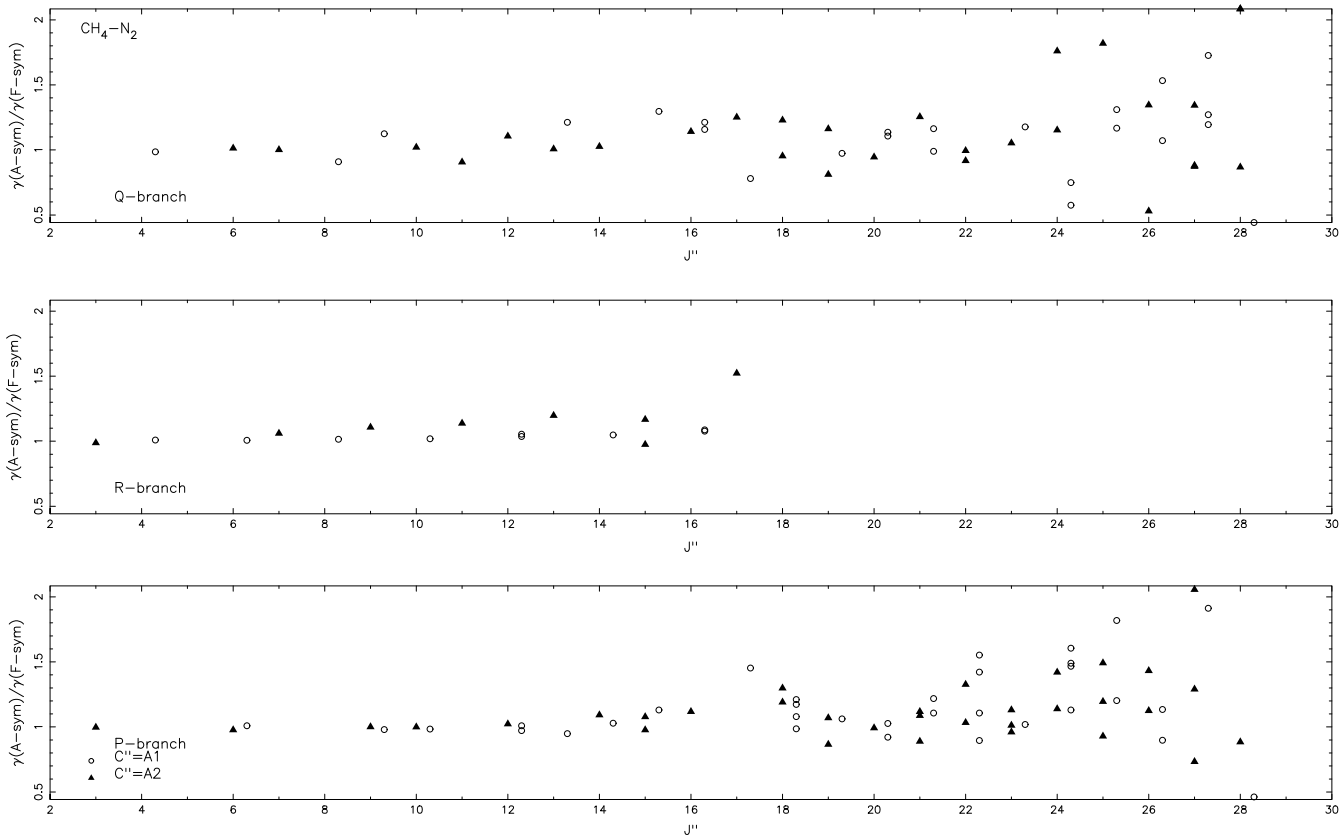

Fig. 2. Ratios of *A*-symmetry transitions to corresponding *F*-symmetry transition versus J''. (Top) *Q*-branch lines, (middle) *R*-branch lines, (bottom) *P*-branch lines. Transitions with $C'' = A1$ are open circles and are shifted to $J'' + 0.3$, transitions with $C'' = A2$ are solid delta symbols.

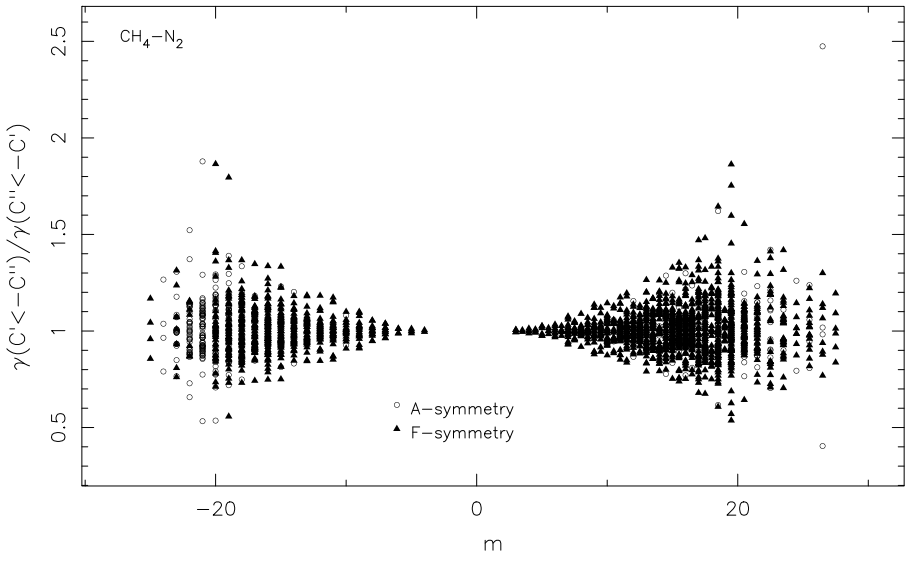

Fig. 3. Ratios of transitions with upper and lower symmetries interchanged versus m where m is $J'' + 0.5$ for *Q*-branch lines, J'' for *R*-branch lines and $-J''$ for *P*-branch lines, *F*-symmetry transitions are solid delta symbols and *A*-symmetry transitions are open circles.

most all the line shifts are negative. Devi et al. [89] also noted that over 95% of their measured line shifts were negative.

4.2. Temperature dependence of the half-width

The solution of the radiative transfer equations for the propagation through the Earth's atmosphere requires that the spectral parameters be known for layers of the atmosphere at different temperatures and pressures. Thus, the knowledge of the temperature dependence of the half-width is essential. Chu et al. [91] have studied the effect of changing the temperature exponent on retrieved mixing ratios of water vapor. They find that changing n from 0.5 to 0.7 results in roughly a 4% change in the mixing ratio at 10 km. It has also been demonstrated that temperature exponents averaged as a function of J'' or fit by polynomials in the rotational quantum numbers do not give reliable predictions for all

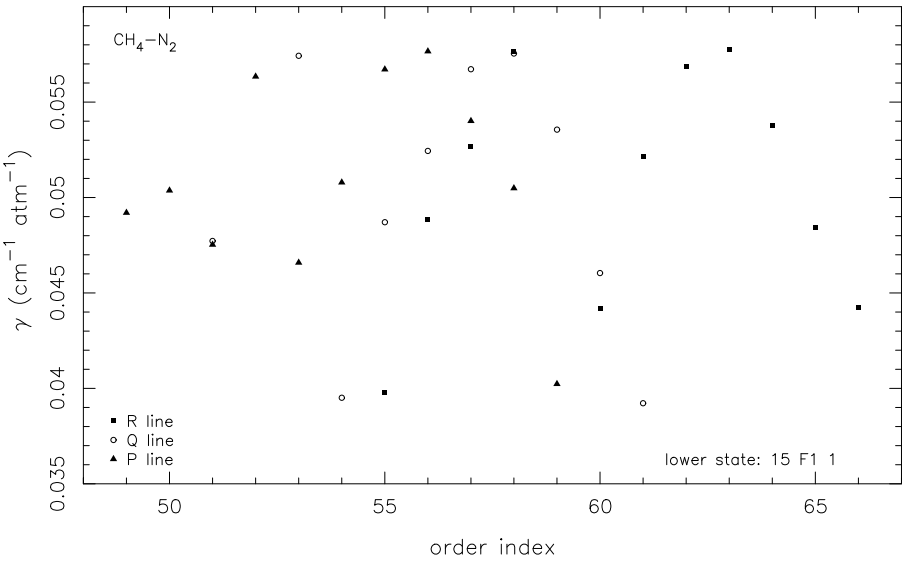

Fig. 4. N_2-broadened half-widths, in units of $cm^{-1}atm^{-1}$, for ν_3 transitions of methane with lower state 15 $F1$ 1. Q-branch lines are open circles, R-branch lines are solid squares, and P-branch lines are solid delta symbols.

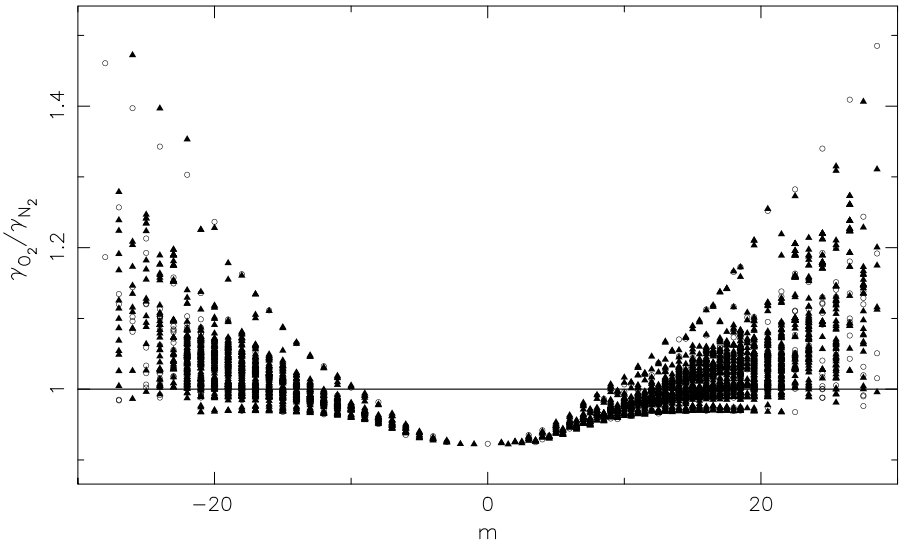

Fig. 5. Ratios of O_2-broadened half-width to corresponding N_2-broadened half-width for ν_3 transitions of CH_4 versus m.

transitions [92,93]. Thus there is a need to know the temperature exponent for many transitions.

As stated earlier, most of the studies that measured the temperature dependence of the half-width used the power-law model, Eq. (10). However, for certain types of radiator-perturber interactions the power law model is being questioned. Wagner et al. [94] have shown that for certain transitions of water vapor perturbed by air, N_2 or O_2 the power law does not correctly model the temperature dependence of the half-width. This fact was also demonstrated by Toth et al. [95] in a study of air-broadening of water vapor transitions in the region from 696 to 2163 cm^{-1}. In both studies it was found that the temperature exponent, n, can be negative for many transitions. In such cases the power law, Eq. (10), is not valid. The mechanism leading to negative temperature exponents was discussed by Wagner et al. [94], by Antony et al. [69], and by Hartmann et al. [96] and is called the resonance overtaking effect.

Here the half-width has been calculated for N_2- and O_2-broadening of 4120 A- and F-symmetry transitions in the ν_3 band at 296 and 225 K. The air-broadened half-width and line shifts were calculated at each temperature using Eq. (9). From these data the temperature exponent of the half-width was determined for each transition for each perturbing gas using Eq. (10). It is thought that Eq. (10) works quite well for ranges in which temperatures vary by only 50–100 K when the major contributions to the half-widths are from the $Re(S_2)$ terms. The model may becomes less valid for large temperature ranges, so one should be cautious in applying Eq. (10) in combustion studies for example. A "rule-of-thumb" expression for the temperature exponent has been given by Birnbaum [97] where the change in the half-width is proportional to $T^{-(m+4)/2m}$. For an "octapole–quadrupole" system, such as CH_4–N_2 or CH_4-O_2, $m = 10$ and the temperature exponent should be 0.7. Here, the values range from a high of around 0.76 to a low of −0.55 (see Table 7). In Fig. 7 the temperature exponents for air-broadening of CH_4 are plotted versus J'' for Q-branch (top panel), R-branch (middle panel), and P-branch (bottom panel) transitions. The F-symmetry transitions are the solid delta symbols and the A-symmetry transitions are the open circle symbols, which are shifted by 0.3 in the

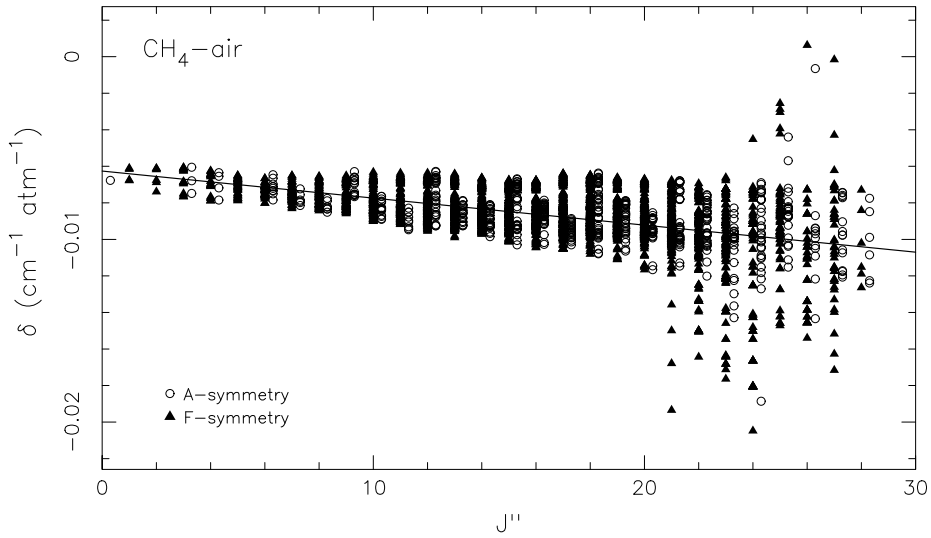

Fig. 6. Air-induced line shifts for ν_3 transitions of methane versus J''. *A*-symmetry transitions are open circles and are shifted to J'' + 0.3, *F*-symmetry transitions are solid delta symbols. Solid line is a straight-line least-squares fit to the data.

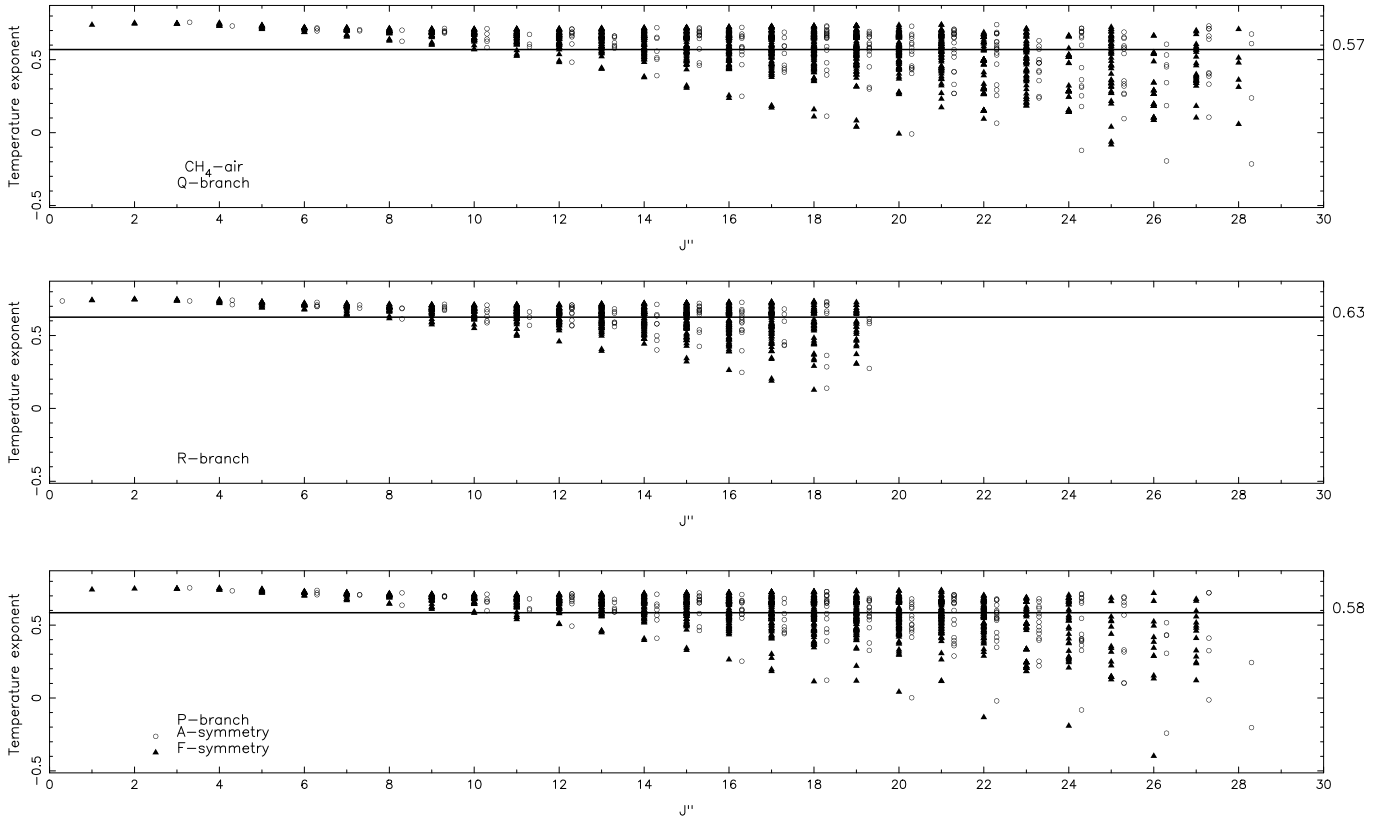

Fig. 7. Temperature exponents for air-broadened half-widths of ν_3 transitions of CH_4 versus J''. (Top) *Q*-branch lines, (middle) *R*-branch lines, (bottom) *P*-branch lines. *A*-symmetry transitions are open circles and are shifted to J'' + 0.3, *F*-symmetry transitions are solid delta symbols. Solid lines are the average temperature exponent for the branch.

x-direction. There appears to be little difference between the branches. The average temperature exponent is 0.57, 0.63, and 0.58 for the *Q*-, *R*-, and *P*-branch transitions, respectively, close to the "rule-of-thumb" value. However, there is considerable spread in the plot and many values are small and some are negative. The studies of Wagner et al. [94] and Antony et al. [69] indicate caution should be exercised when using Eq. (10) for the collision systems studied here. The fact that many values of the temperature exponent are small or negative suggests that the temperature dependence should be examined more closely. The results of Mondelain et al. [24] also suggest the power law model may not be the best for methane. Here, the values were determined by two points, hence the correlation coefficient of the fit to Eq. (10) could not be made. The fits should be redone with many points to address the validity of the power law. This work is in progress.

Table 8
Comparison of measured half-widths with CRB calculations for ν_3 transitions of methane

System	Measurement	No. of lines	Average percent different	Standard deviation (%)
CH_4–N_2	[44]	52	0.15	4.9
	[45]	85	−4.6	14.7
	[46]	80	−2.4	4.9
	[47]	82	−0.84	6.4
	[48]	52	−1.3	4.7
	[24]	4	−2.8	3.9
CH_4–O_2	[44]	52	−2.1	4.7
	[45]	72	−4.0	11.2
CH_4–air	[50]	3	1.5	—
	[45]	131	−3.0	13.4

4.3. Comparison with measurement

The calculations of the half-widths for the *A*- and *F*-symmetry ν_3 transitions of CH_4 at 296 K made here were compared to the corresponding N_2-, O_2-, and air-broadening measurements [24,34,44–48,50]. Note that Refs. [44,46–48] are measurements of the same lines with different line shape models. Below we compare with each but in the comparison with all measurements in the ν_3 band we exclude the data from Refs. [47,48] and when only a few lines were measured [34,50]. Table 8 gives the average percent difference and standard deviation between the CRB calculations and measurement for ν_3 lines considered in this study. There are a good number of measurements of N_2-broadening of ν_3 transitions of methane. Here we are able to compare with 221 transitions giving a −2.7 percent difference with a standard deviation of 10.0. If we look at the data of Pine without various line shape models the percent difference between measurement and the CRB calculations is −0.15 [44] and −2.4 [46], both with a standard deviation of 4.9. In Fig. 8 the measured N_2-broadened half-widths and the CRB calculated half-widths are plotted versus *m*. The measurements are Ref. [44] *A*-species solid circle, *F*-species open circle, [46] *A*-species solid square, *F*-species open square, [45] *A*-species solid delta symbol, *F*-species open delta symbol, and [24] *A*-species solid star symbol, *F*-species open star symbol. It is apparent that there is some spread in the measurements. The calculations appear to track the measurements fairly well. In Fig. 9 the percent difference between the CRB calculations and the N_2- [44,46] and the O_2-broadening [44] data of Pine are plotted versus *m*. *A*-symmetry lines are the open circles and *F*-symmetry lines are the solid delta symbol. We note in the figure that more *A*-symmetry lines have negative percent differences whereas the F-symmetry lines are more evenly distributed between plus and minus.

Table 9 gives the average ratio of the measured line shift divided by the calculated line shift for N_2-, O_2-, and air-broadening of ν_3 transitions of methane. In all cases the ratios are below 1, indicating the calculations are too large in magnitude. In the calculations the line shift is strongly dependent on the vibrational dependence of the polarizability. Here the *ab initio* values of Raynes et al. [76] have been used, which come from a calculation of the polarizability surface using a Hartree–Fock wavefunction. It is clear that the calculations would benefit from adjusting this parameter to match the measurements.

The calculated temperature dependence of the half-width can be compared with the measurements of Varanasi [50] (three lines), Devi et al. [34] (three lines), and Mondelain [24] (four lines). These comparisons are presented in Table 10. In all but the $R(0)$ line measured by Varanasi the calculated values are smaller than the measured values. The calculations presented here are the mean-relative thermal velocity approximation to the CRB equations. It has been shown in the case of water vapor [94] and ozone [98] that the velocity integral form of the CRB equations gives better results for the temperature dependence of the half-width. This will be a topic of a future study.

5. Conclusions

Calculations of the pressure-broadened half-width, the pressure induced line shift, and the temperature dependence of the half-width have been made for nitrogen-, oxygen-, and air-broadening of ν_3 transitions of CH_4 in the 2726 to 3200 cm^{-1} region of the spectrum. The calculations were made at two temperatures, 225 and 296 K, and for rotational states with $J \leqslant 28$. Because of limitations in the current codes only *A*- and *F* symmetry transitions were considered. Calculations were made for 4120 *A*- and *F*- symmetry transitions in this region. The final list of transitions is comprised

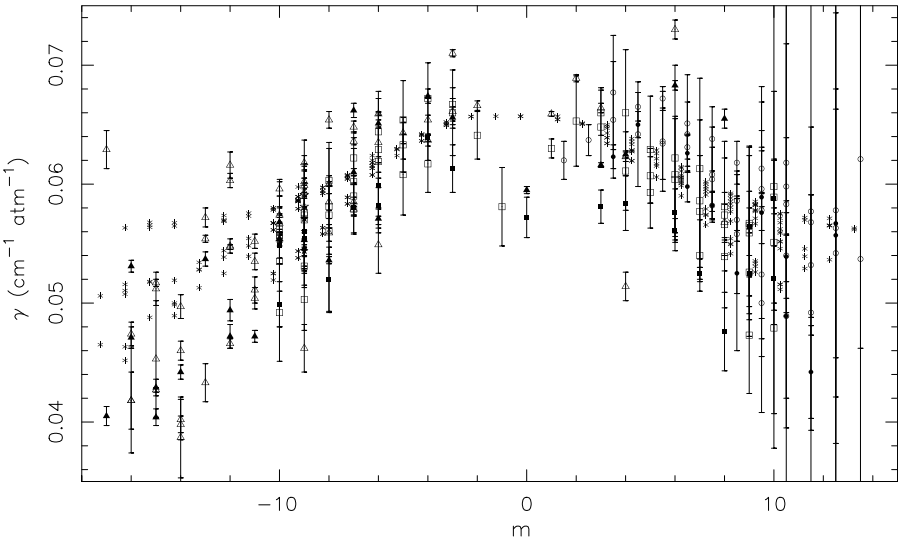

Fig. 8. Measured N_2-broadened half-widths with error bars and the CRB calculated half-widths (∗ symbol) are plotted versus *m*. The measurements are Ref. [44] *A*-species solid circle, *F*-species open circle, Ref. [46] *A*-species solid square, *F*-species open square, Ref. [45] *A*-species solid delta symbol, *F*-species open delta symbol, and Ref. [24] *A*-species solid star symbol, *F*-species open star symbol.

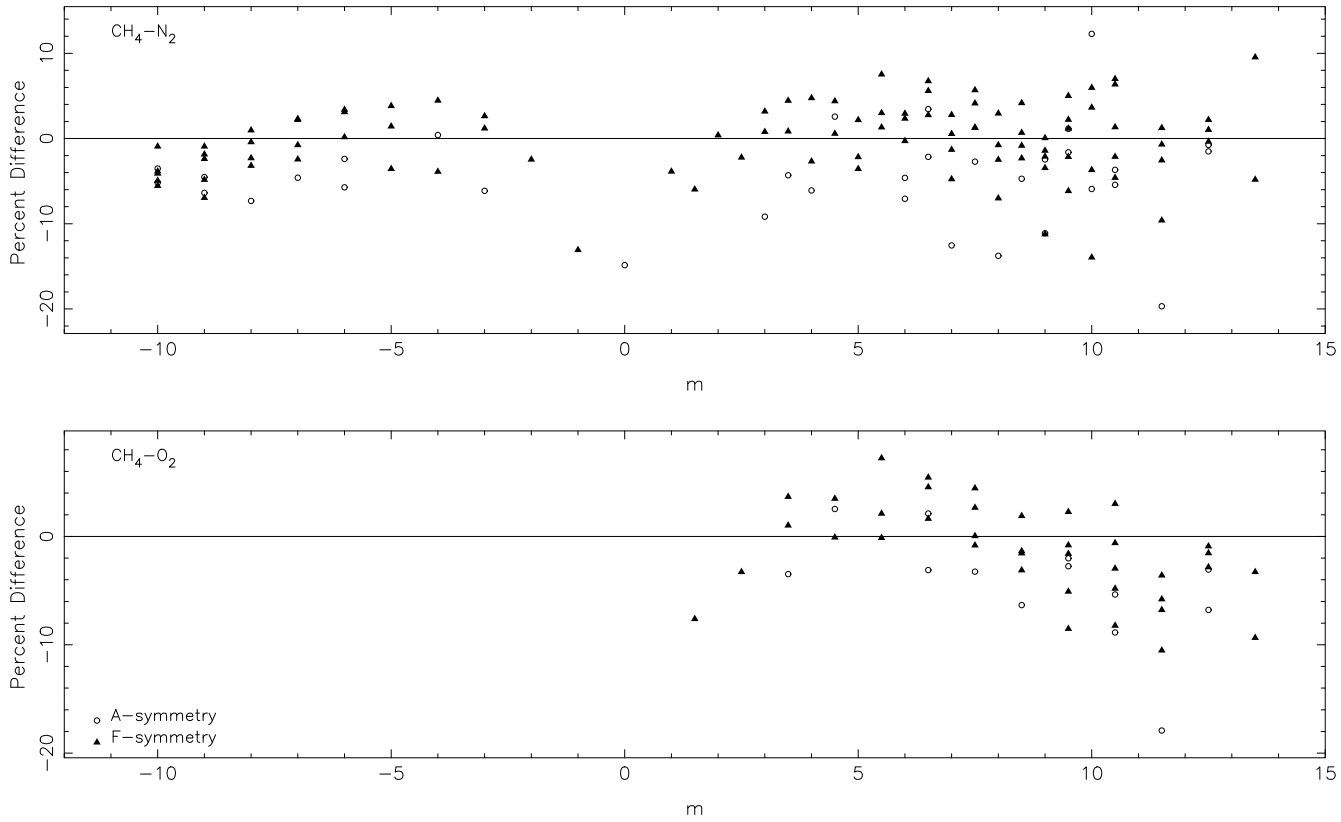

Fig. 9. Percent difference between the CRB calculations and the N_2-broadening [44,46] and the O_2-broadening [44] data of Pine versus *m*. *A*-symmetry lines are the open circles and *F*-symmetry lines are the solid delta symbol.

Table 9
Comparison of measured line shifts with CRB calculations for ν_3 transitions of methane

System	Measurement	No. of lines	Ave($\delta_{exp}/\delta_{CRB}$)
CH_4–N_2	[44]	52	0.69
	[45]	85	0.59
CH_4–N_2	[46]	80	0.75
	[47]	82	0.77
	[48]	52	0.71
CH_4–O_2	[44]	52	0.76
	[45]	72	0.70
CH_4–air	[45]	131	0.66

Table 10
Comparison of measured temperature dependence of the half-width with CRB calculations for ν_3 transitions of methane

Ref.	Perturber	Transition	n_{exp}	n_{CRB}
[50]	Air	1 *A*2 3 ← 0 *A*1 1	0.62	0.737
		2 *F*2 10 ← 1 *F*1 1	1.0	0.742
		3 *F*1 13 ← 2 *F*2 1	1.0	0.748
[34]	N_2	13 *A*2 19 ← 14 *A*1 1	0.995(17)	0.515
		13 *F*2 53 ← 14 *F*1 1	0.975(32)	0.527
		13 *F*1 54 ← 14 *F*2 2	0.944(30)	0.495
[24]	N_2	8 *A*1 12 ← 9 *A*2 1	0.836(35)	0.689
		8 *F*1 32 ← 9 *F*2 2	0.841(14)	0.689
		8 *F*2 33 ← 9 *F*1 3	0.858(12)	0.689
		8 *A*2 10 ← 9 *A*1 1	0.839(35)	0.695

of 524 *A*-symmetry transitions and 3596 *F*-symmetry transitions. The calculations did not take into account any line coupling effects. From the calculations the temperature dependence of the nitrogen-, oxygen-, and air-broadened half-widths were determined.

The CRB results for the half-widths compared with measurements of Pine [44,46] give reasonable percent differences and standard deviations. However, Mondelain et al. [24] have demonstrated that retrievals of methane volume mixing ratios from balloon spectra made using slightly different line shape parameters show noticeable effects. Some researchers [99] are dismayed at the state of methane-broadening parameters with the HITRAN database having measurements for a few thousand transitions and bad estimates (±20%) for the remaining 480 000 transitions [31]. Thus our calculations are not yet at the level desired by all researchers for terrestrial atmospheric applications but certainly are an improvement of the estimated values. The accuracies needed for Titan remote sensing are less stringent (5–10%) and the CH_4–N_2 calculations presented here meet that criterion. The comparisons for the line shifts were not as good. This may be due in part to the magnitude of the parameter as well as the uncertainty in the parameters used in the calculation (vibrational-dependence of the polarizability of methane and the atom-atom coefficients).

While the agreement with the measured data of Pine gives good statistics (see above) the differences vary between roughly ±10% with a few stray points. The fact that the calculations cannot yet be done for *E*-symmetry transitions is also of concern. In the future we will investigate the form of intermolecular potential used in the calculations and the parameters used with emphasis on reducing the spread in the agreement with Pine and being able to compute E-symmetry transitions as well. We also have wavefunctions for ν_4 states, which will allow us to consider vibration dependence of the half-widths and line shifts from calculations of ν_3 and ν_4 transitions. When this is accomplished the calculations can be extended to other broadening species such as H_2 and He.

The final air-broadened data file was given to Dr. Larry Rothman to be merged with the measured half-widths for addition to the HITRAN database. From the measurements cited above it would seem reasonable to replace the estimated half-widths on HITRAN with the calculated ones independent of vibrational band and isotopolog.

Files and plots for all perturbers considered here are available from one of the authors (R.R.G., http://faculty.uml.edu/Robert_Gamache) and the data files are available as supplementary files.

Acknowledgments

The authors are pleased to acknowledge support of this research by the National Aeronautics and Space Administration (NASA) through Grant No. NAG5-11064 and by the National Science Foundation (NSF) through Grant No. ATM-0242537. Any opinions, findings, and conclusions or recommendations expressed in this material are those of the author(s) and do not necessarily reflect the views of NASA or NSF.

Appendix A. Supplementary data

Supplementary data for this article are available on ScienceDirect (www.sciencedirect.com) and as part of the Ohio State University Molecular Spectroscopy Archives (http://library.osu.edu/sites/msa/jmsa_hp.htm). Supplementary data associated with this article can be found, in the online version, at doi:10.1016/j.jms.2008.03.012.

References

[1] J.F.B. Mitchell, C.J. T, J.M. Gregory, S.F.B. Tett, Nature 376 (1995) 501–504.
[2] S.F.B. Tett, P.A. Stott, M.R. Allen, W.J. Ingram, J.F.B. Mitchell, Nature 399 (1999) 569–572.
[3] W.S. Broecker, Science 278 (1997) 1582–1588.
[4] P.U. Clark, N.G. Pisias, T.F. Stocker, A.J. Weaver, Nature 415 (2002) 863–869.
[5] L. Marshall, J.J. Jung, J. Derber, M. Chahine, R. Treadon, S.J. Lord, M. Goldberg, W. Wolfc, H.C. Liu, J. Joiner, J. Woollen, R. Todling, P. van Delst, Y. Tahara, Bull. Am. Meteorol. Soc. 87 (2006) 891–894.
[6] M.I. Hegglin, P.F. Bernath, C.D. Boone, W.H. Daffer, P. Hoor, G.L. Manney, C. Schiller, K. Strong, K.A. Walker, Atmos. Chem. Phys. Discuss. 7 (2007) 13861–13882.
[7] R. Nassar, P.F. Bernath, C.D. Boone, G.L. Manney, S.D. McLeod, C.P. Rinsland, R. Skelton, K.A. Walker, Geophys. Res. Lett. 32 (2005) L15S04.
[8] C.P. Rinsland, P.F. Coheur, H. Herbin, C. Clerbaux, C. Boone, P. Bernath, L.S. Chiou, J. Quant. Spectros. Radiat. Transfer 107 (2007) 340–348.
[9] C.P. Rinsland, M. Luo, M.W. Shephard, C. Clerbaux, C.D. oone, P.F. Bernath, L. Chiou, P.F. Coheur, J. Quant. Spectros. Radiat. Transfer, in press.
[10] H. Fischer, M. Birk, C. Blom, B. Carli, M. Carlotti, T. von Clarmann, L. Delbouille, A. Dudhia, D. Ehhalt, M. Endemann, J.M. Flaud, R. Gessner, A. Kleinert, R. Koopmann, J. Langen, M. Lopez-Puertas, P. Mosner, H. Nett, H. Oelhaf, G. Perron, J. Remedios, M. Ridolfi, G. Stiller, R. Zander, Atmos. Chem. Phys. Discuss. 7 (2007) 8795–8893.
[11] J. Kar, H. Bremer, J.R. Drummond, Y.J. Rochon, D.B.A. Jones, F. Nichitiu, J. Zou, J. Liu, J.C. Gille, D.P. Edwards, M.N. Deeter, G. Francis, D. Ziskin, J. Warner, Geophys. Res. Lett. 31 (2004) L23105.
[12] A.G. Straume, H. Schrijver, A.M.S. Gloudemans, S. Houweling, I. Aben, A.N. Maurellis, A.T.J. de Laat, Q. Kleipool, G. Lichtenberg, R. van Hees, J.F. Meirink, M. Krol, Adv. Space Res. 36 (2005) 821–827.
[13] A. Bracher, H. Bovensmann, K. Bramstedt, J.P. Burrows, T. von Clarmann, K.-U. Eichmann, H. Fischer, B. Funke, S. Gil-López, N. Glatthor, U. Grabowski, M. Höpfner, M. Kaufmann, S. Kellmann, M. Kiefer, M.E. Koukouli, A. Linden, M. López-Puertas, G.M. Tsidu, M. Milz, S. Noel, G. Rohen, A. Rozanov, V.V. Rozanov, C. von Savigny, M. Sinnhuber, J. Skupin, T. Steck, G.P. Stiller, D.-Y. Wang, M. Weber, M.W. Wuttke, Adv. Space Res. 36 (2005) 855–867.
[14] D. Blumstein, G. Chalon, T. Carlier, C. Buil, P. Hebert, T. Maciaszek, G. Ponce, T. Phulpin, B. Tournier, D. Simeoni, P. Astruc, A. Clauss, G. Kayal, R. Jegou, M. Strojnik (Eds.), IASI Instrument: Technical Overview and Measured Performances, in: Proceedings of SPIE, vol. 5543, Infrared Spaceborne Remote Sensing XII, 2004.
[15] G. Chalon, F. Cayla, D. Diebel, IASI : An Advance Sounder for Operational Meteorology, in: Proceedings of the 52nd Congress of IAF, Toulouse, France, 2001.
[16] J.A. Griggs, J.E. Harries, J. Climate 20 (2007) 3982–4001.
[17] G.C. Toon, J.-F. Blavier, B. Sen, J.J. Margitan, C.R. Webster, R.D. May, D. Fahey, R. Gao, L.D. Negro, M. Proffitt, J. Elkins, P.A. Romashkin, D.F. Hurst, S. Oltmans, E. Atlas, S. Schauffler, F. Flocke, T.P. Bui, R.M. Stimpfle, G.P. Bonne, P.B. Voss, R.C. Cohen, J. Geophys. Res 104 (1999) 26. 779–726, 790.
[18] D.J.W. Kendall, T.A. Clark, Appl. Opt. 18 (1979) 346–353.
[19] F. Friedl-Vallon, G. Maucher, M. Seefeldner, O. Trieschmann, A. Kleinert, A. Lengel, C. Keim, H. Oelhaf, H. Fischer, Appl. Opt. 43 (2004) 3335–3355.
[20] M.B. Esler, D.W.T. Griffith, S.R. Wilson, L.P. Steele, Anal. Chem. 72 (2000) 206–215.
[21] R.A. Washenfelder, G.C. Toon, J.-F. Blavier, Z. Yang, N.T. Allen, P.O. Wennberg, S.A. Vay, D.M. Matross, B.C. Daube, J. Geophys. Res. 111 (2006) D22305.
[22] D.W.T. Griffith, FTIR measurements of atmospheric trace gases and their fluxes, in: J.M. Chalmers, P.R. Griffiths (Eds.), Handbook of Vibrational Spectroscopy, John Wiley and Sons, New York, 2002, pp. 2823–2841.
[23] C. Senten, M.D. Mazière, B. Dils, C. Hermans, M. Kruglanski, E. Neefs, F. Scolas, A.C. Vandaele, G. Vanhaelewyn, C. Vigouroux, M. Carleer, P.F. Coheur, S. Fally, B. Barret, J.L. Baray, R. Delmas, J. Leveau, J.M. Metzger, E. Mahieu, C. Boone, K.A. Walker, P.F. Bernath, K. Strong, Atmos. Chem. Phys. Discuss. 8 (2008) 827–891.
[24] D. Mondelain, S. Payan, W. Deng, C. Camy-Peyret, D. Hurtmans, A.W. Mantz, J. Mol. Spectrosc. 244 (2007) 130–137.
[25] A. Coustenis, R.K. Achterberg, B.J. Conrath, D.E. Jennings, A. Marten, D. Gautier, C.A. Nixon, F.M. Flasar, N.A. Teanby, B. Bézard, R.E. Samuelson, R.C. Carlson, E. Lellouch, G.L. Bjoraker, P.N. Romani, F.W. Taylor, P.G.J. Irwin, T. Fouchet, A. Hubert, G.S. Orton, V.G. Kunde, S. Vinatier, J. Mondellini, M.M. Abbas, R. Courtin, Icarus 189 (2007) 35–62.
[26] F.M. Flasar, R.K. Achterberg, B.J. Conrath, P.J. Gierasch, V.G. Kunde, C.A. Nixon, G.L. Bjoraker, D.E. Jennings, P.N. Romani, A.A. Simon-Miller, B. Bézard, A. Coustenis, P.G.J. Irwin, N.A. Teanby, J. Brasunas, J.C. Pearl, M.E. Segura, R.C. Carlson, A. Mamoutkine, P.J. Schinder, A. Barucci, R. Courtin, T. Fouchet, D. Gautier, E. Lellouch, A. Marten, R. Prangé, S. Vinatier, D.F. Strobel, S.B. Calcutt, P.L. Read, F.W. Taylor, N. Bowles, R.E. Samuelson, G.S. Orton, L.J. Spilker, T.C. Owen, J.R. Spencer, M.R. Showalter, C. Ferrari, M.M. Abbas, F. Raulin, S. Edgington, P. Ade, E.H. Wishnow, Science 308 (2005) 975–978.
[27] V.G. Kunde, F.M. Flasar, D.E. Jennings, B. Bézard, D.F. Strobel, B.J. Conrath, C.A. Nixon, G.L. Bjoraker, P.N. Romani, R.K. Achterberg, A.A. Simon-Miller, P. Irwin, J.C. Brasunas, J.C. Pearl, M.D. Smith, G.S. Orton, P.J. Gierasch, L.J. Spilker, R.C. Carlson, A.A. Mamoutkine, S.B. Calcutt, P.L. Read, F.W. Taylor, T. Fouchet, P. Parrish, A. Barucci, R. Courtin, A. Coustenis, D. Gautier, E. Lellouch, A. Marten, R. Prangé, Y. Biraud, C. Ferrari, T.C. Owen, M.M. Abbas, R.E. Samuelson, F. Raulin, P. Ade, C.J. Césarsky, K.U. Grossman, A. Coradini, Science 305 (2004) 1582–1586.
[28] A. Barbe, in: Proceedings of the Atmospheric Spectroscopy Applications Workshop, ASA REIMS 96, Université de Reims, Champagne Ardenne, 1996.
[29] L.S. Rothman, D. Jacquemart, A. Barbe, D.C. Benner, M. Birk, L.R. Brown, M.R. Carleer, C. Chackerian Jr., K. Chance, L.H. Coudert, V. Dana, V.M. Devi, J.-M. Flaud, R.R. Gamache, A. Goldman, J.-M. Hartmann, K.W. Jucks, A.G. Maki, J.-Y. Mandin, S.T. Massie, J. Orphal, A. Perrin, C.P. Rinsland, M.A.H. Smith, J. Tennyson, R.N. Tolchenov, R.A. Toth, J. Vander Auwera, P. Varanasi, G. Wagner, J. Quant. Spectrosc. Radiat. Transfer 96 (2005) 139–204.
[30] L.R. Brown, J. Quant. Spectros. Radiat. Transfer 96 (2005) 251–270.
[31] L.R. Brown, D.C. Benner, J.P. Champion, V.M. Devi, L. Fejard, R.R. Gamache, T. Gabard, J.C. Hilico, B. Lavorel, M. Loete, G.C. Nikitin, A.S. Pine, A. Predoi-Cross, C.P. Rinsland, O. Robert, R.L. Sams, M.A.H. Smith, S.A. Tashkun, V.G. Tytuterev, J. Quant. Spectrosc. Radiat. Transfer 82 (2003) 219–238.
[32] P. Varanasi, J. Quant. Spectros. Radiat. Transfer 11 (1971) 1711–1724.
[33] K. Fox, D.E. Jennings, E.A. Stern, R. Hubbard, J. Quant. Spectros. Radiat. Transfer 39 (1988) 473–476.
[34] V.M. Devi, B. Fridovich, G.D. Jones, D.G.S. Snyder, J. Mol. Spectrosc. 97 (1983) 333–342.
[35] P. Varanasi, L.P. Giver, F.P.J. Valero, J. Quant. Spectrosc. Radiat. Transfer 30 (1983) 481–490.
[36] V.M. Devi, B. Fridovich, D.G.S. Snyder, G.D. Jones, P.P. Das, J. Quant. Spectrosc. Radiat. Transfer 29 (1983) 45–47.
[37] K. Fox, D.E. Jennings, J. Quant. Spectrosc. and Radiat. Transfer 33 (1985) 275–280.
[38] V.M. Devi, C.P. Rinsland, M.A.H. Smith, D.C. Benner, Appl. Opt. 24 (1985) 2788–2791.
[39] C.E. Keffer, C.P. Conner, W.H. Smith, J. Quant. Spectros. Radiat. Transfer 35 (1986) 495–499.
[40] C.P. Rinsland, V.M. Devi, M.A.H. Smith, D.C. Benner, Appl. Opt. 27 (1988) 631–651.
[41] P. Varanasi, S. Chudamani, J. Quant. Spectros. Radiat. Transfer 41 (1989) 335–343.
[42] P. Varanasi, S. Chudamani, J. Quant. Spectros. Radiat. Transfer 43 (1990) 1–11.
[43] M.A.H. Smith, C.P. Rinsland, V.M. Devi, D.C. Benner, Spectrochim. Acta 48A (1992) 1257–1272.
[44] A.S. Pine, J. Chem. Phys. 97 (1992) 773–785.
[45] D.C. Benner, V.M. Devi, M.A.H. Smith, C.P. Rinsland, J.Quant. Spectrosc. Radiat. Transfer 50 (1993) 65–89.
[46] A.S. Pine, J. Quant. Spectrosc. Radiat. Transfer 57 (1997) 157–176.
[47] A.S. Pine, T. Gabard, J. Quant. Spectros. Radiat. Transfer 66 (2000) 69–92.
[48] A.S. Pine, T. Gabard, J. Mol. Spectrosc. 217 (2003) 105–114.
[49] D. Mondelain, P. Chelin, A. Valentin, D. Hurtmans, C. Camy-Peyret, J. Mol. Spectrosc. 233 (2005) 23–31.
[50] P. Varanasi, J. Quant. Spectrosc. Radiat. Transfer 15 (1975) 281.
[51] V.M. Devi, D.C. Benner, M.A.H. Smith, C.P. Rinsland, J. Mol. Spectrosc. 157 (1993) 95–111.

[52] V.M. Devi, D.C. Benner, M.A.H. Smith, C.P. Rinsland, J. Quant. Spectros. Radiat. Transfer 51 (1994) 439–465.
[53] A. Predoi-Cross, M. Brawley-Tremblay, L.R. Brown, V.M. Devi, D.C. Benner, J. Mol. Spectrosc. 236 (2006) 201–215.
[54] R.L. Barger, J.L. Hall, Phys. Rev. Lett. 22 (1969) 4–8.
[55] G. Hubbert, T.G. Kyle, G.F. Troup, J. Quant. Spectros. Radiat. Transfer 9 (1969) 1469–1476.
[56] D.H. Rank, U. Fink, T.A. Wiggins, Astrophys. J. 143 (1971) 980–988.
[57] J.S. Margolis, J. Quant. Spectros. Radiat. Transfer 11 (1971) 69–73.
[58] P. Varanasi, G.D.T. Tejwani, J. Quant. Spectros. Radiat. Transfer 12 (1972) 849–855.
[59] J. Ballard, W.B. Johnston, J. Quant. Spectros. Radiat. Transfer 36 (1986) 365–371.
[60] A. Predoi-Cross, L.R. Brown, V.M. Devi, M. Brawley-Tremblay, D.C. Benner, J. Mol. Spectrosc. 232 (2005) 231–246.
[61] C.P. Rinsland, V.M. Devi, M.A.H. Smith, D.C. Benner, Appl. Opt. 28 (1989) 2111–2118.
[62] D. Robert, J. Bonamy, J. Phys. 20 (1979) 923–943.
[63] R.R. Gamache, R. Lynch, S.P. Neshyba, J. Quant. Spectrosc. Radiat. Transfer 59 (1998) 319–335.
[64] S.P. Neshyba, R. Lynch, R.R. Gamache, T. Gabard, J.-P. Champion, J. Chem. Phys. 101 (1994) 9412–9421.
[65] R.R. Gamache, R. Lynch, J. Quant. Spectrosc. Radiat. Transfer 64 (2000) 439–456.
[66] R.R. Gamache, N. Lacome, G. Pierre, T. Gabard, J. Mol. Struct. 599 (2001) 279–292.
[67] J.F. Brian, J. Drouin, Robert R. Gamache, J. Quant. Spectrosc. Radiat. Transfer 83 (2004) 63–81.
[68] R.R. Gamache, J.-M. Hartmann, J. Quant. Spectrosc. Radiat. Transfer 83 (2004) 119–147.
[69] B.K. Antony, S. Neshyba, R.R. Gamache, J. Quant. Spectrosc. Radiat. Transfer 105 (2006) 148–163.
[70] L.R. Brown, C.M. Humphrey, R.R. Gamache, J. Mol. Spectrosc. 246 (2007) 1–21.
[71] R. Lynch, R.R. Gamache, S.P. Neshyba, J. Quant. Spectrosc. Radiat. Transfer 59 (1998) 595–613.
[72] R. Lynch. Half-widths and Line Shifts of Water Vapor Perturbed by Both Nitrogen and Oxygen. Ph.D. dissertation, Physics Department, University of Massachusetts Lowell, June, 1995.
[73] P.W. Anderson, Phys. Rev. 76 (1949) 647–661.
[74] C.J. Tsao, B. Curnutte, J. Quant. Spectrosc. Radiat. Transfer 2 (1962) 41–91.
[75] R. Kubo, J. Phys. Soc. Jpn. 17 (1962) 1100–1120.
[76] W.T. Raynes, P. Sazzeretti, R. Zanazi, Mol. Phys. 64 (1988) 1061–1071.
[77] J.E. Jones, Proc. R. Soc. A 106 (1924) 463–477.
[78] J.O. Hirschfelder, C.F. Curtiss, R.B. Bird, Molecular Theory of Gases and Liquids, Wiley, New York, 1964.
[79] R.J. Good, C.J. Hope, J. Chem. Phys. 55 (1971) 111–116.
[80] R.A. Sack, J. Math. Phys. 5 (1964) 260–268.
[81] S.P. Neshyba, R.R. Gamache, J. Quant. Spectrosc. Radiat. Transfer 50 (1993) 443–453.
[82] J.-P. Champion, M. Löete, G. Pierre, Spherical top spectra, in: K.N. Rao, A. Weber (Eds.), Spectroscopy of the Earth's Atmosphere and Interstellar Medium, Academic Press, Inc., USA, 1992, pp. 339–422.
[83] V. Boudon, J.-P. Champion, T. Gabard, M. Löete, F. Michelot, G. Pierre, M. Rotger, Ch. Wenger, M. Rey, J. Mol. Spectrosc. 228 (2004) 620–634..
[84] J.-P. Champion, G. Pierre, F. Michelot, J. Moret-Bailly, Can. J. Phys. 55 (1977) 512–520.
[85] T. Gabard, J.-P. Champion, J. Quant. Spectros. Radiat. Transfer 52 (1994) 303–317.
[86] T. Gabard, J. Quant. Spectrosc. Radiat. Transfer 57 (1997) 177–196.
[87] A. Predoi-Cross, A.V. Unni, H. Heung, V.M. Devi, D.C. Benner, L.R. Brown, J. Mol. Spectrosc. 246 (2007) 65–76.
[88] V.M. Devi, Private Communication, The College of William and Mary, Wiliamsburg, VA, 1988.
[89] V.M. Devi, D.C. Benner, M.A.H. Smith, C.P. Rinsland, Appl. Opt. 30 (1991) 287–304.
[90] G.T.D. Tejwani, P. Varanasi, K. Fox, J. Quant. Spectros. Radiat. Transfer 15 (1975) 243–254.
[91] W.P. Chu, E.W. Chiou, J.C. Larsen, L.W. Thomason, D. Rind, J.J. Buglia, S. Oltmans, M.P. McCormick, L.M. McMaster, J. Geophys. Res. 98 (1993) 4857–4866.
[92] R.R. Gamache, S.P. Neshyba, J.J. Plateaux, A. Barbe, L. Régalia, J.B. Pollack, J. Mol. Spectrosc. 170 (1995) 131–151.
[93] R.R. Gamache, R. Lynch, L.R. Brown, J. Quant. Spectros. Radiat. Transfer 56 (1996) 471–487.
[94] G. Wagner, M. Birk, R.R. Gamache, J.-M. Hartmann, J. Quant. Spectrosc. Radiat. Transfer 92 (2005) 211–230.
[95] R.A. Toth, L.R. Brown, M.A.H. Smith, V. Malathy Devi, D. Chris Benner, M. Dulick, J. Quant. Spectrosc. Radiat. Transfer 101 (2006) 339–366.
[96] J.M. Hartmann, J. Taine, J. Bonamy, B. Labani, D. Robert, J. Chem. Phys. 86 (1987) 144–156.
[97] G. Birnbaum, Adv. Chem. Phys. 12 (1967) 487–548.
[98] J.-M.C. Dominique Priem, François Rohart, Georges Wlodarczak, R.R. Gamache, J. Mol. Spectrosc. 204 (2000) 204–215.
[99] R.A. Washenfelder, P.O. Wennberg, G.C. Toon, Geophys. Res. Lett. 30 (2003) 2226.
[100] C.G. Gray, J. Phys. B 4 (1971) 1661–1669.
[101] D.R. Lide (Ed.), CRC Handbook of Physics and Chemistry, 83rd ed., The Chemical Rubber Company, Clevland, OH, 2003.
[102] G. Birnbaum, E.R. Cohen, J. Chem. Phys. 62 (1975) 3807–3812.
[103] F. Mulder, G. Van Dijk, A. Van Der Avoird, Mol. Phys. 39 (1980) 407–425.
[104] K.P. Huber, G. Herzberg, Molecular Spectra and Molecular Structure: Constants of Diatomic Molecules, Van Nostrand, New York, 1979.
[105] M.P. Bogaard, B.J. Orr, in: A.D. Buckingham (Ed.), MPT International Review of Science, Physical Chemistry, Series Two, Molecular Structure and Properties, vol. 2, Butterworth, London, 1975 (chapter 5).
[106] A. Lofthus, The molecular spectrum of nitrogen, Department of Physics, University of Oslo, Blindern, Norway, Spectroscopic Report No. 2, vol. 1, 1960.
[107] D.E. Stogryn, A.P. Stogryn, Mol. Phys. 11 (1966) 371–393.